RADIOGRAPHY WITH HEAVY PARTICLES*

E. V. Benton; R. P. Henke

Physics Department
University of San Francisco

C. A. Tobias; M. R. Cruty

Donner Laboratory
Lawrence Berkeley Laboratory

August, 1975

*Work in part sponsored by NCI Contract #YO1-CB-40302, with BEVALAC beam time supplied by ERDA.

Abstract

The failure of X-ray diagnostic techniques to accurately detect tumors and other regions of abnormal density in soft tissue has been, for many years, a significant shortcoming of this important technique in medicine. Accelerated heavy particles with plastics for track detection can be used to record small differences in density in soft tissues which may correspond to biological structures and abnormalities. In heavy-particle radiography (HPR), plastic detectors are well suited for recording images since their threshold nature makes them insensitive to spurious low-LET radiations and light secondaries. Sources of error which limit the resolution of HPR are inversely dependent on the atomic mass number (A) of the incident particle. Range straggling, responsible for loss of depth resolution, is proportional to $A^{-0.5}$ while multiple scattering which degrades lateral resolution is approximately proportional to $A^{-0.395}$. Recent experiments showing calcification in human blood vessels and soft tissue features in rats underline the potential of HPR as a diagnostic tool. High-resolution, three-dimensional reconstructions are possible using multiple layer plastic detectors; the short exposure time produces blur-free radiographs of specimens whose internal structure may be in motion.

Table of Contents

I. Introduction

Our interest in particle radiography was generated during the planning of a biomedical accelerator, in 1967. At that time it was suggested that a number of existing problems in diagnostic roentgenology might be solved through the use of energetic particle beams (1); among those problems are:

1. Soft-tissue abnormalities and tumors are often not detectable with X-rays or other conventional techniques. A tumor is detected by X-rays generally only when it has grown to a rather large size.
2. In some cases air or a radio-opaque substance must be injected in order to detect certain soft-tissue regions such as the third ventricle. Such localization might be accomplished without injections if heavy particles are used.
3. Internal blood clots are not easy to detect. Since the density of these is often greater than that of surrounding tissue, they might be visualized with heavy particle beams.
4. When small density differences must be detected, as in mammography, the need for very soft X-rays results in undesirably high doses.

Imaging in diagnostic X-ray radiography depends largely on differences in absorption between different tissues. Absorption in turn depends on atomic absorption coefficients. In many instances with X-rays, there is no resolution of an abnormal soft tissue region, even though this region may be well differentiated from the biological point of view, if its absorption coefficient is similar to that of the surrounding tissue. In such cases a much more sensitive detection of this slight difference in specimen composition is afforded by using the variation of the stopping power of the specimen to accelerated heavy particles rather than the variation in the

X-ray absorption coefficient (2). This increased resolution derives from the fact that the ionization produced by a particle beam varies from a small value to its maximum value for a displacement of the beam stopping point of only the order of 1% of the range of the beam, where the range of the beam must only slightly exceed the thickness of the specimen. On the other hand in conventional diagnostic X-ray radiography, the electromagnetic radiation must be able to penetrate the entire specimen and still retain adequate intensity to sufficiently expose the film without giving unduly high radiation dose to the entrance side of the specimen; in this case the distance scale for a large variation in the X-ray radiation intensity must be the order of the thickness of the specimen. Consequently heavy particle radiography affords a sensitivity increase of the order of 100-fold in cases where the percentage change in the particle stopping power is the same as the percentage change in the X-ray absorption coefficient.

In addition to the significantly higher sensitivity, particles afford several other advantages over X-rays; these advantages are that:

1. the measurement of the residual range of fast particles after they have crossed the body can also be used for determining the three-dimensional density distribution inside.
2. particle radiography can be done with a much lower patient dosage than received with X-rays.
3. diagnostic pictures can be obtained during very short time intervals that eliminate blurring due to motion.

Experimental efforts in particle radiography began in 1968 with Lyman's attempts in three-dimensional proton laminography of a phantom. At the same time Koehler, et al (3) (4) (5) began work on proton techniques, which have produced very interesting pictures. Related work by West, et al has likewise produced interesting results (6) (7). In a recent paper (8) and

report (9) it was shown that the use of monoenergetic oxygen particles produced in the Berkeley Bevatron, in combination with thin-sheet plastic track detectors, will considerably extend the possibility of detecting soft-tissue abnormalities and localizing air pockets. These results suggested that heavier particles have a greater diagnostic potential than protons.

From the mathematical analysis developed by Goitein (10) for use in Lyman's investigation, it became apparent that three-dimensional reconstruction of proton densitograms might be a very important diagnostic tool and an adjunct to therapy*. Subsequently Budinger (12) developed the mathematical physics and computer techniques for 3-D reconstruction from multiple 2-D views for use in both emission and transmission studies in nuclear medicine and electron microscopy; these techniques are directly applicable to proton or heavy particle radiography. Another reconstruction technique has been developed by New, et al in conjunction with the EMI scanner (20).

Biological research with high-energy accelerated deuterons, protons and helium ions began in Berkeley more than 20 years ago; the first human therapeutic exposures with these particles began at this time. Recently, two accelerators were combined to form a single multipurpose heavy-ion accelerator, the BEVALAC; this unique machine is a national facility (21). Since the use of heavy particles in contrast to protons should result in better depth and lateral resolution because of the decrease in range straggling and scattering with increasing atomic mass, the BEVALAC is eminently suitable for a comparative evaluation of the use of protons and of heavier ions in diagnostic radiology.

In this report we shall discuss the particle and beam parameters which affect image resolution in particle radiographs together with the results of some preliminary heavy particle exposures. The theory and the preliminary

*A status report on this work is available (11).

results present a strong case for the use of heavy particles over protons for diagnostic radiography and of particles over X-rays for resolution of features which differ only slightly in density and/or composition from surrounding material.

II. Physical Aspects of Particle Radiography

The basic elements of any radiographic technique are resolution (longitudinal, lateral, volume) and patient dosage. In particle radiography these elements are a function of the physical interactions between beam particles and the target, characteristics of the particle beam, and the type of particle track detector which is used for imaging. Before we can discuss the effects of these aspects on the above elements, it is first necessary to briefly discuss the aspects themselves. To this end we shall outline, in this section, the pertinent physical considerations which are involved in the particle radiographic technique. The remaining two aspects are discussed in the subsequent two sections.

A charged particle of a particular atomic number, Z, atomic weight, A, and energy, E, will penetrate a given absorber to some precisely known depth called the range, R*. Consequently, a beam of monoenergetic charged particles will stop in a homogeneous absorber at approximately the same depth. For example, Figure 1 shows a proton attenuation curve determined for a graphite absorber, showing that most of the particle attenuation comes with a thickness change of about 5%. If the range of the incident particles is adjusted to be nearly the same as the thickness of the radiographed object, a small change in the thickness or density of the object will result in a relatively large change in the number of particles that penetrate the object. By placing a suitable detector downstream of the object to record the emerging particles, high sensitivity to changes in thickness or density is achieved. The variation in recorded track density constitutes the radiographic image of the object. The quality of the image is dependent on certain physical factors. Among the most important of these are:

---

*See Appendix A for a discussion of range-energy relationships.

A. Range Straggling.

As an energetic, charged nuclear particle penetrates matter it loses energy primarily through interaction with the electrons in the stopping medium. Since the number of energy transfers to electrons is finite, there is a statistical fluctuation of the particle ranges due to the randomness of the energy transfers. This variation in the ranges of particles with the same incident energy is known as range straggling. The range straggling of various ions in water is shown as a function of the particle range in Figure 2. The values are computed from the work of Barkas (13) in emulsion scaled to other materials using Equation 5.66 of Burcham (14). The straggling is expressed as the standard deviation of the longitudinal stopping-point distribution. The curves in Figure 2 can be represented very accurately by the analytical formula,

$$\sigma_R = 0.0120\ R^{0.951}A^{-0.5} \quad (cm) \tag{1}$$

It can be seen that the standard deviation of range straggling, σ_R is almost proportional to range, R, and is inversely proportional to the square root of the atomic mass number, A.

Straggling is the dominant limitation of depth resolution in particle radiography. The thicker parts of the human body are equivalent to 30-40 cm water in their stopping power; the range straggling of protons at that thickness is about 1.00% of the range while straggling for helium ions is about half that for protons; for accelerated carbon ions it is only 0.29% of the range.

B. Multiple Scattering.

As energetic nuclear particles are brought to rest by electrons, they also interact elastically with the nuclei of the atoms in the stopping

material. While very little energy is exchanged in these nuclear interactions, the moving particle is deflected from its original direction of travel, usually through a very small angle. The cumulative effect of many of these very small deflections is known as multiple scattering of the particle. If many particles with identical trajectories and range (R) in water are stopped by traveling through a single homogeneous stopping material (with no air spaces), the standard deviation of the lateral distribution of the stopping points is approximately given by the relation:

$$\sigma_X = 0.0232\ Z^{-0.207}\ A^{-0.396}\ R^{0.896}\ Z_s^{0.963}\ A_s^{-0.5} \qquad (2)$$

where Z_s and A_s are the atomic number and atomic mass number of the stopping material, and R and σ_X are given in cm. Equation (2) is obtained from Eqn. (13.111) of Jackson (15)* using the range energy relationship [Equation (A-1) in Appendix A] to obtain "pv". A factor of 1/2 converts $\langle\theta^2\rangle$ to its projected value and the factor of distance to the stopping point squared is the lever arm factor which converts the increment of σ_θ^2 into an increment of σ_X^2. The logarithmic term is replaced by a power function approximation and the expression then integrated from the radiographed feature to the beam stopping point. The contribution to σ_X by the material upstream from the radiographed feature is not included in Equation (2). The values of σ_X given by Equation (2) are shown in Figure 3. As in the case of range straggling, it can be seen that there is a strong dependence on the atomic number of the incident particle. For a given particle range, there is a much smaller spread in the lateral positions of the stopping points for heavier particles.

From the point of view of multiple scattering, accelerated carbon particles thus present a gain of about four-fold over protons in resolving

---

*$\langle\theta^2\rangle \simeq 4\pi N \left(\frac{2Z\ z_s e^2\ 2}{(\ pv\ )}\right) \ln(210 Z_s^{-1/3}) t$ where t is the thickness of material containing N atoms per unit volume.

details of a linear tissue structure; with respect to resolving an area, the gain is 16-fold.

C. Inelastic Collisions.

Some of the particles suffer inelastic collisions in passing through matter. These particles are deflected or lost from the beam producing one or more secondary recoil particles in tissue at the site of the collision. The cross section (6) for this scattering process is

$$\sigma = \pi R_o^2 \, (A^{1/3} + M^{1/3} - 1.17)^2 \qquad (3)$$

where R_o is the radius of a proton, A the mass number of the accelerated particle and M the mass number of the absorber. The formula is due to Bradt and Peters; refinements have been made here on the basis of recent accelerator data.

When the accelerated particles are protons, the beam attenuation by this process is relatively small. However, with increasing atomic number, the loss of particles from the beam becomes substantial, making it inadvisable to use very heavy particles for tissue radiography. The secondary particles cause an increased spread of a portion of the beam and add to background. While some of the detection techniques (e.g. plastic detectors, see below) minimize this effect because their efficiency is much lower for the lighter secondaries, the lost particles must be compensated for by the use of an increased particle flux. Another effect of inelastic collisions is that the nuclear disintegrations produced add to the dose received by the patient. However this is a very small effect and does not unduly increase dosages received by patients.

D. Air Spaces.

Perfect lateral resolution would be achieved if all particles in a parallel beam which pass through a given point on the radiographed object also stop at the same lateral position on the detector. The real situation deviates from this ideal situation because of three factors: 1) inherent, accelerator-produced angular dispersion of the particle trajectories at points in the beam, 2) additional angular dispersion produced by multiple scattering, and 3) the path length through which the particles travel beyond the target before coming to rest, which transforms the angular dispersion into a lateral spatial dispersion. The accelerator-produced angular dispersion is relatively minimal. As the beam comes to rest it inescapably suffers multiple scattering which becomes more and more pronounced as the particles' momenta decrease and the momentum transfers in collisions with nuclei become greater.

The mean deflection of particles from straight line trajectories remains relatively small as long as the particles have high energy and travel continuously in dense media. When particles emerge from dense medium to air, particularly at lower energies where the angular dispersion has become large, the lateral deviation from straight-line trajectory increases markedly, causing a deterioration in the ability to resolve structures in the radiographed object. This effect is due to the fact that the trajectories of scattered particles have an angular distribution and that, in air, large distances are traversed without a corresponding change in the beam energy. This effect is qualitatively demonstrated in Figure 4.

The scattering angle, lateral spread and loss of resolution in air are markedly smaller with heavy ions than with protons.

For optimal resolution in particle radiography it is advisable to leave little or no air space between subject and the detector.

E. Abrupt Density Change or Phase Change.

Small-angle multiple scattering of heavy particles can give rise to edge pattern near sharp interfaces between objects when there is an abrupt density change; a similar effect is used in zerography techniques of diagnostic radiology with X-rays. West and Sherwood of the Harwell laboratories (6, 7) recently analyzed this effect by the use of protons. We believe that this effect was observed in one of the radiographs taken with an oxygen beam at the Bevatron.

Since the r. m. s. multiple scattering angle changes approximately as $1/\sqrt{A}$, where A is the mass of the particle, heavy ions are better than protons for scattering radiography. The difference results in better resolution and in the ability to resolve structure in thicker objects at the same kinetic energy of the particles.

III. Accelerator Beam Aspects of Particle Radiography

There are several properties of accelerated beams which can modify the effectiveness of particle radiography. Among these are:

A. Energy spread.

The desired depth resolution for particle radiography is about 0.2 to 0.3%. In order to achieve this, it is necessary to use discrete particle energies that correspond to the thickness and stopping power of the object to be radiographed. Equally important, the particles must have a very small energy spread after they emerge from the accelerator.

The range energy curve in Figure 5 indicates the energies necessary for complete passage of the particles through subjects of various dimensions. In the Bevatron/Bevalac it will be possible to choose appropriate energies at any level above 100 MeV/nucleon by timing of the deflection mechanism. The maximum energy spread in a single pulse with this machine is about 0.5%. The use of fast carbon and oxygen beams has resulted in deflected beams with much smaller energy spread.

The energy spread of helium ions and protons in the 184" cyclotron is about 0.5%, so that pictures taken at this machine at the present time would have poorer resolution than those taken at the Bevatron. However, at the expense of intensity reduction, it may be possible to reduce energy spread in the cyclotron also.

B. Angular Divergence.

Most of the beams extracted form accelerators show, in addition to energy spread, angular convergence and divergence of the particles. It is

desirable to reduce this lack of uniform direction of the particles to such a level that the resolving power achieved would not be affected by this factor.

The Bevalac beam-focusing channels are arranged in such a manner that monoenergetic particles can be brought to a near focus. By applying 0.5 cm aperture in the focal plane a distance (D) of 5 meters or more between focal plane and radiographic setup, the beam divergence (θ_B) can be kept to one milliradian or less. Since such a divergence will cause an error in image resolution of less than 0.03 cm, it might be necessary to have an evacuated space between focal spot and subject in order to keep air scattering to minimum. Beam emittance is 30 mm-mradian lateral and 60 mm-mradian vertical.

C. Spherical Correction.

The use of focused beams would cause the endpoints of the ranges of particles crossing a slab of matter of uniform density not to lie in a plane surface, but instead these would be on a curved surface. A local region of a few cm^2 of a radiograph would not be appreciably affected by this factor. However, when large size (e.g. 50 cm x 50 cm) radiographs are processed, it might be necessary to apply corrections as part of computerized handling of data or place a thin energy degrader of the shape of convex optical lens midway between the focus and the detectors to produce a planar stopping distribution.

D. Timing and Particle Flux.

Most of the components of soft tissues are in constant motion, due to the beating of the heart, breathing, peristaltic motion, muscle-twitch background, etc. Some believe that these motions are sources of errors and of

lack of resolution in conventional X-ray soft tissue radiography.

The Bevalac delivers pulsed beams. It is a built-in feature of this machine that pulses are obtainable in controlled time sequence from a few microseconds upward to a few tenths of a second. Since there is sufficient particle flux in a single pulse for a radiograph of 10^{-3} or 10^{-4} second duration, this may allow synchronization of the radiographs to motion sequences of the body. It is possible that some cyclotrons might also be programmed in an appropriate manner for this purpose.

Radiographs of good quality require uniform beam-density distribution over the object to be radiographed. Because of the complicated beam dynamics in the accelerators, this represents special technical problems; a radiographic detector system under construction will also be used to adjust accelerator parameters for optimal uniformity of the beam density.

IV. Detector Characteristics and Response in Particle Radiography

A general requirement for a detection system in a new radiographic method is that the system should be able to record an optimum portion of the information carried by the diagnostic particle beam. There should be a minimum of time delay introduced by the detector system; its background should be low and the radiation dose to the patient should be minimized. Additional desirable features include low cost, ability to conveniently store the information and a format accessible for computer processing of the data. We consider two systems briefly: plastic nuclear track detectors and photographic film.

A. Plastic Nuclear Track Detectors.

Plastic nuclear track detectors record the passage of charged particles if the ionization rate of the particles (LET = linear energy transfer)* exceeds the critical value that is characteristic of the particular detector (16, 17, 18). The two most commonly used plastic detectors are cellulose nitrate and Lexan polycarbonate with the former being considerably more sensitive. The detector development consists of a chemical treatment in a strong hydroxide solution (e.g. 6.25N NaOH) which results in the preferential chemical etching of the radiation-damaged material along the particle trajectory. In this way, a microscopically observable "track" is produced.

The plastic nuclear track detector response can be characterized by the chemical etch rate along the particle trajectory (V_T), as a function of the particle-restricted energy loss rate (LET) (17). For normally incident

*The response of plastic nuclear track detectors more closely follows the LET_{350} rather than LET_∞ of particles. This is why the quantity LET_{350} is used throughout this work. Over a wide range of particle velocities LET_{350} can be converted to LET_∞ by multiplying by a factor of ~ 1.6.

tracks, a very good approximation to the Lexan detector response and a reasonably good approximation to the cellulose nitrate (CN) detector response is given by:

$$V_T = \begin{cases} V_G & \text{for } LET_{350} < LET_{crit} \\ V_G \left[\frac{LET_{350}}{LET_{crit}}\right]^{\psi} & \text{for } LET_{350} \geq LET_{crit} \end{cases} \quad (4)$$

where V_G is the bulk etch rate of the detector surface. For Lexan (without UV sensitization), $LET_{crit} \simeq 300$ KeV/μ (H_2O) and $\psi \simeq 2$. For CN, $LET_{crit} \simeq 80$ keV/μ (H_2O) and $\psi \simeq 4$. It can be seen that the CN is much more sensitive than Lexan.

Two significant aspects of the plastic response can be seen from Equation 4. First, the threshold nature of the detection implies that no particle tracks will be produced if the particle range in the detector is greater than a registration range, R_{reg}, derived from the values of LET_{crit}. Second, the track etch rate, hence the track size and the macroscopically observable response, increases rapidly as the particle stopping point is approached and LET_{350} increases. This places the effective response point very close to the particle stopping point, particularly in the case of Lexan. In fact, it occurs at a residual range of somewhat less than $R_{reg}/2$, the effective response range for detectors with constant response in the region $LET_{350} > LET_{crit}$. For example, $R_{reg} \simeq 0.014$ cm (H_2O) for ^{16}O in Lexan.

It is important to compute the detector response curve as a function of the distance from the nominal particle stopping point. This is accomplished by convoluting the stopping-point distribution with the detector response as a function of residual range. For example, the familiar Bragg curve results when the detector is an ionization chamber. Here, the detector response is the total particle ionization. In Figures 7 and 8 are shown

the normalized Lexan and CN response curves as a function of the water-equivalent distance from the nominal stopping point. Here the Lexan response is taken to be the total track opening area on both surfaces of the detector. This should approximate the macroscopic response given by observing the layers with scattered light (dark field illumination). An experimental demonstration of the Lexan response curve is shown in Figure 6, which shows an etched Lexan stack which has been separated to reveal the individual layers.

In Figure 7, two response curves are shown for the CN detector. One gives the response as seen by light transmitted through the central opening areas of tracks etched completely through the plastic. The other gives the response that would be obtained by counting the tracks (which is a large task for large numbers of detector layers or particle radiographs with much detail). The assumed amount of surface bulk etch for the central opening area response is only 8.6μ. For longer etch times, the central opening curve will approach the track count curve in appearance.

It can be seen that the Lexan response curve approximates the particle stopping-point distribution quite well, The track hole opening area CN response curve has approximately the same width as the stopping-point distribution, even though it is shifted slightly upstream. These threshold detectors can therefore be assumed to be measuring the stopping-point distribution without introducing any more than a negligible amount of longitudinal spread.

An exposed plastic nuclear track detector preserves an image of the distribution of heavy particles stopping in it in the form of a hole or cone distribution. This image can be transformed to photographic film by transilluminating the plastic film by light of appropriate wavelength.

The distribution is also suitable for further computer processing: the plastic sheets are automatically scanned by a suitable device and the co-ordinates where tracks are located are transferred to computer tape or memory.

A very attractive feature of plastic nuclear track detectors is the fact that every stopping particle is recorded.

B. Photographic Film.

Photographic films are generally used in diagnostic radiology and their characteristics are well known. Both have been used in our study, for evaluation of their suitability in proton and heavy-ion radiography, and for comparative diagnostic pictures taken by X-ray. However, it appears that there are several disadvantages:

1. Without intensifying screen, X-ray films need relatively large dose in terms of particle flux density. Approximately 10^6 protons cm^{-2} are needed for good contrast, causing a dose of about 0.03 rad to 3 rad in tissue at various energies.
2. When intensifying screens are used, these are likely to decrease depth variation.
3. The film response is logarithmical and the background noise on the film is relatively large. Photographic film is sensitive not only to protons but also to electrons and electromagnetic radiation.
4. It is relatively difficult to compare two films of the same subject because photographic development introduces general changes in tone and contrast. For similar reasons, transfer of the film information to computer is not very practical.

C. Comparison of Plastics and Photographic Film for Track Registration in HPR.

We have recently carried out experiments which clearly show that high-resolution, high-contrast radiographs can be produced utilizing heavy-particle beams in conjunction with either photographic film or plastic nuclear track detectors (8, 9). The emphasis has been on using plastics in that they offer some unique advantages over the photographic film. For this purpose, the main limitations of the photographic emulsions consist of the following; emulsions record heavy particles over their entire trajectory; they record electrons producing an unwanted "halo" effect, and they record all charged secondaries. Also, since plastic detectors record tracks only at the end of the particle range, it is possible to detect very small variations in the stopping power of the object. Since each layer of a stack of exposed plastics may have unique thickness information recorded on it, it then becomes possible to construct a two-dimensional map of the thickness of the target object.

The contrast between conventional, i.e. "X-ray radiography", and heavy-particle radiography with plastic detectors is illustrated in Figure 9. Here the X-ray mean free path length and the heavy-particle range are the same. The X-ray intensity (the processed film reproduces this intensity) and the Lexan response to the heavy-ion beam are normalized to one at their peak values. As the tissue composition changes, the water-equivalent path length for either absorption or stopping varies with lateral position in the beam. As can be seen from the figure, the resulting fractional change in Lexan response, $\Delta R_T/R_T$ is much greater than the fractional change in the X-ray intensity, $\Delta I_x/I_x$. The "noise" with plastic detectors is generally very low and typically represents the development of a small density of background etch pits as well as the fragment-induced tracks. Consequently it appears

that plastics are more suitable for heavy particle radiography than are photographic films. However, more rigorous comparative studies are planned.

V. Basic Elements of Particle Radiography

Having presented selected pertinent physical, beam, and detector aspects of particle radiography, we are now in a position to discuss the effect of these aspects on the basic elements of particle radiography, i.e., resolution (longitudinal, lateral, volume) and dosage.

A. Longitudinal (Depth) Resolution.

Four factors combine to determine the change in subject thickness that can be diagnostically measured These are: range straggling, initial beam energy spread, range shortening due to multiple scattering, and errors involved in determining the range of a group of particles in the detector. We believe that the last two factors can be made much smaller than the first two, so that, for relatively large regions, the r.m.s. deviation in range measurement, δ_R, can be expressed as:

$$\delta_R \approx (\delta^2_{\text{Range spread}} + \delta^2_{\text{straggling}})^{1/2}$$

By purifying the beam so that its energy spread is less than 0.1%, we are left with straggling as the essential variable.

Heavy particles are the best suited to high-depth resolution because they have much smaller values of range straggling than light particles, as can be seen in Figure 2. Because of the smaller range straggling, heavy particles indicate the average value of the stopping point much more accurately than light particles. Moreover, plastics are the ideal detecting material because of their threshold registration characteristics, recording particles only very near their stopping point. Thus, the relatively narrow stopping region of the heavy particles is well localized. For more sensitive

detectors, such as film, which record the particles at great distances from their stopping points, much of the information about those particles stopping near the detector is obscured by the particles stopping farther downstream, which are also recorded. Therefore, the downstream stopping-point displacements do not produce the desired reduction in intensity on the detector.

If we quantitatively define the depth resolution by requiring that the displacement in the average particle stopping distance be detectable at least at the one standard deviation level for each point of a 10 x 10 raster (100 points/feature) across the feature to be resolved, the required particle fluence (F) is given by:

$$F > \frac{0.0144\ R^{1.902}}{A_f\ t^2\ (\Delta f)^2\ A} \qquad (5)$$

where all units are cgs units. In Equation (5), R is the range of the full-energy particles, A_f and t are the area and thickness of the feature to be detected, Δf is the change in stopping-power conversion factor between the feature and the surrounding medium, and A is the atomic mass number of the incident particle. The factor f is the relative stopping power in the region of interest as compared with the energy loss rate in water. Equation (5) is derived using Equation (1) and by assuming that all particle stopping points are determined. The error (standard deviation) of the stopping point determination is then $\sigma_R/\sqrt{0.01\ A_f\ F}$, which is equated to one to obtain Equation (5). Some of the possible features of interest and their values of f are given in Table 1.

Table 1.

STOPPING-POWER CONVERSION FACTORS

Stopping material	f
water (tissue)	1.00
tumor[1]	1.05
bone	1.8
air	0.001

[1]The density factor of 1.05 is given here for illustrative purposes only. Initial, unpublished measurements in our Laboratory indicate that, for soft-tissue tumors, this factor varies from 0.95 to 1.05.

As an example of the application of Equation (5), we calculate the particle fluence necessary to resolve a 1-cm diameter spherical tumor immersed in normal tissue. If this is located in the torso, the particles must have a range of the order of 50 cm. The area of the tumor is 0.785 cm^2 and its average thickness is 0.667 cm. Δf is 1.05 - 1.00 = 0.05. Therefore,

$$F = \frac{0.0144 \times 50^{1.902}}{0.785 \times 0.667^2 \times 0.05^2 A} = \frac{28{,}000}{A}$$

If protons are used (A = 1), 28,000 particles/cm^2 will be required. If Ar particles are used (A = 40), 700 particles/cm^2 will be required to resolve the tumor (neglecting losses due to nuclear interaction).

It is of interest to compute the smallest feature that can be detected with a given particle fluence. If we assume spherical features with diameter d (cm), then, for track registration, it is necessary that:

$$d > \frac{0.451\ R^{0.476}}{(\Delta f)^{0.5}\ (AF)^{0.25}}$$

For example, with a particle fluence of 10^4 particles/cm^2 and R = 50 cm, air bubbles (Δf = 1) can be resolved if:

$$d > 0.29\ A^{-0.25}$$

This means that bubbles 0.29 cm in diameter can be resolved with protons, and those 0.12 cm in diameter can be resolved with Ar particles.

B. Lateral Resolution.

The theoretical evaluation of lateral resolution is not a perfectly straightforward procedure, due to the fact that it is very dependent on the image-processing techniques that are applied to the radiograms. It is also true that the lateral resolution is not independent of the depth resolution. This can be seen by the factor A_f in Equation(5). As a first approximation it is reasonable to assume that the limiting lateral resolution cannot be much less than the standard deviation of the lateral distribution of stopping points produced by multiple scattering and given by Equation(2). It is expected that even computer enhancement of the image cannot improve the lateral resolution limit given by Equation(2)by more than a factor of two.

The lateral resolution appears to be the limiting factor in heavy-particle radiography. For example, protons can depth resolve an air bubble 0.29 cm in diameter on the upstream side of the torso (see previous example). However, Figure 3 shows that an air bubble 1.39 cm in diameter is required for lateral resolution.

An evaluation of the relative lateral resolution capabilities of various particles at various ranges in water can then be seen by considering Figure 3. For example, Ar particle beams should register objects which are approximately eight times as small in linear dimensions as objects that can be resolved with a proton beam. For the thinner regions of the radiographed subject, it should be possible to achieve much greater resolution than for the thick regions if the beam energy is reduced.

C. Volume Resolution.

Combining depth resolution and area resolution, it seems clear that heavy particles can resolve substantially smaller volume features than protons. For helium ions vs. protons, the ratio is about 8; for carbon ions vs. protons about 64; and for argon vs. protons, even greater. By increasing the fluence of protons and using computing aids, proton resolution is somewhat improved. However, in each instance, heavier ions give greater contrast than protons for the same objects viewed.

D. Dose.

There are several factors that affect the dose: 1) the particles' energy loss rate, 2) the particle fluence (particles per unit area), 3) range straggling, and 4) nuclear disintegrations that have taken place upstream from the point where the dose is to be evaluated. If we are dealing with beams with reasonably low initial energies so nuclear disintegrations can be neglected, and if we are evaluating the dose at a point somewhat removed from the stopping point of the particles, a reasonably accurate evaluation of the dose can be obtained by considering only the particle energy loss rate and the particle fluence. The deposited energy density in MeV/cm^3 is given by the fluence, F, times LET_∞, as given by Equation (A-2)*. This can be converted to dose in rads through multiplying by the appropriate conversion factors necessary to obtain the units of 100 ergs/gm. For water (or tissue) the approximate dose (D) in rads is then given by:

$$D = 2.85 \times 10^{-7} Z^{1.207} (A/R)^{0.396} F \qquad (8)$$

where R is in cm of water. Equation (8) should only be applied when R is greater than 1 cm and less than approximately 50 cm.

---

*Appendix A.

The values of the dose are presented in Figure 10 for a particle fluence of 1000 particles/cm^2. It can be seen that, for this fluence, and even at 1 cm for Ar, the dose is quite low in comparison to the normal chest X-ray. Particle fluences as high as 10^4 particles/cm^2 for Ar and 10^6 particles/cm^2 for protons appear usable, even though they may not be required since lateral resolution is the primary limiting factor in resolution.

When protons are used instead of carbon particles, dose in rads remains the same or possibly higher than for carbon. One reason is that more protons must be used per feature in order to obtain resolution.

The total number of particles in a beam remains quite low, even if large radiographs are made. For example, a 50 cm x 50 cm carbon radiograph, with 1000 particles per cm^2, would use only 2.5×10^5 particles. This is several orders of magnitude lower than can be delivered by the BEVALAC in a single pulse.

VI. Preliminary Results of our HPR Technique

Results of our initial work in heavy-particle radiography (HPR) appear in References (8) and (9). Recently, several additional experiments were conducted. The following is a brief description of this unpublished work.*

A test of longitudinal resolution was carried out using a piece of Lucite with grooves of varying depths cut into the block. Beams of ^{12}C and ^{16}O were used and recorded by stacks of Lexan. In Figure 11 are shown photographs of the Lucite resolution tester and two layers of processed Lexan, one each from the ^{12}C and ^{16}O exposures. The fifth groove from the left having a depth of 0.2 mm can clearly be observed in each case. A much better depth resolution can be achieved through actual counting of tracks in the regions of interest. It should be noted also that this and the subsequent radiographs were produced by having the particle beam first traverse approximately 10 cm of water.

A test of lateral resolution was carried out using a piece of aluminum having variable depth and spacing of triangular grooves, as shown in Figure 12a. Radiographs were obtained using beams of ^{16}O particles recorded by stacks of Lexan and cellulose nitrate. In Figure 12b is shown an edge view of a processed cellulose nitrate stack which illustrates well the three-dimensional character of the recorded image. The white outline of the grooves in aluminum represents the position in the detector stack where the particle beam came to rest. The appearance of one sheet of this stack is shown in Figure 12c. As before, a true test of resolution would involve track counting in the areas of interest.

A combined test of lateral and longitudinal resolution involved the use

*A disclosure of invention was made to the AEC Patent Division by C. A. Tobias and E. Benton. This matter is currently being handled by the Patent Office, Univ. of California, Berkeley (AEC Case No. S-43, 158(RL-5951; IB-140)).

of a model of a tumor as shown in Figure 13a. Here, a 1-cm cavity in a block of Lucite was filled with a 5% lower stopping power sucrose solution. Numerous small air bubbles were allowed to remain between the two halves of the block sealed by means of a 0.5 mm piece of polyethylene plastic. In Figures 13b and 13c are shown two Lexan radiographic layers produced by a beam of ^{12}C particles. The images of all of the air bubbles are clearly recorded including the smallest bubble which is about 1 mm in diameter. Again it should be noted that the object is overlaid by a 10-cm thick layer of water. Figures 13d through 13g are Lexan radiographic layers with the 1 cm cavity filled with sucrose solutions whose stopping powers are 2%, 3%, 4%, and 5% lower than Lucite, respectively.

Figure 14 shows a ^{16}O-produced, cellulose nitrate radiographic sequence of a diseased human aorta with an X-ray appearing on the bottom right. The dark areas appearing on the X-ray are areas of calcification. The particle-plastic radiographs show the calcification in considerably more detail; this may be another area where HPR can make an important contribution.*

In all cases, the above radiographs were obtained by using a single beam pulse of about 10^6 particles, spread to an area of about 40 cm^2, corresponding to an absorbed dose of about 0.1 rad. Lower exposure levels (about 0.01 rad) still yielding high-quality radiographs can be obtained by enlarging the recorded tracks through a longer etch time. Since exposure times are very short and can be varied down to about 1 microsecond through control of the deflection system, the technique can also be applied to obtain blur-free radiographs of biological specimens in motion.

Our latest work was the imaging of a 150 gram F344 rat using 400 MeV/amu neon particles from the BEVALAC. For this exposure the beam was

---

*This work was performed by D. Cafiso as an undergraduate thesis in Biophysics, University of California, Berkeley, 1974. It is on file with the Medical Physics Division, Donner Laboratory, UC, Berkeley.

spread to a diameter of roughly 16 inches. Particle fluences of 10^4, 10^5, 10^6, and 10^7 particles cm^{-2} were used, respectively, with 9" x 12" x 0.4" stacks of alternate layers of Lexan and red-tinted cellulose nitrate for track registration.

The rat was sacrificed approximately twelve hours before exposure, and three 1/4" x 1/4" right cylinders of polystyrene (density: $\sim$ 1.04 gr cm^{-3}; stopping power: $\sim$ 1.08 times that of H_2O) were implanted. The implants were in the right thigh, on the left side, and beneath the diaphragm, with the rat viewed abdomen up. Metal sutures were used to close the incisions and to serve as reference points. The rat was then tied to a support frame and refrigerated at just above 32^oC. For the exposure the rat/frame assembly was immersed in a 12" x 12" x 2" Lucite water bath. Detector stacks were positioned against the downstream face of the water tank.

Figure 15a through Figure 15j is a sequence of Lexan radiographs of the rat from a fluence of 10^5 particles cm^{-2}; the layer in Figure 15a lies closest to the rat. Denser features such as bone, are imaged earliest in the sequence; organs such as the liver and stomach become visible later. What is most interesting about the radiographs is the sharpness (or contrast) of various interfaces. Figure 16 is a radiographic image of the rat in cellulose nitrate from the same detector stack as Figures 15a to 15; Figure 17 is an X-ray of the same rat done in air.

It is clear from the work to date that HPR is a viable imaging technique, although more work is needed to optimize the images and refine their interpretation. Application of reconstruction techniques to multiple views should greatly extend the amount and quality of information which can be obtained.

VII. Conclusion

In about one year the relative merit of protons, helium ions and heavier particles for diagnosis, as far as the physical factors of depth and lateral resolution, contrast and type of detector systems are concerned should be known. Within two years it should be possible to obtain a clear indication of the subfields of cancer diagnosis where the techniques might be useful. Should particle radiography extend the ability of radiologists in early and accurate diagnosis of cancer as we expect, then it is logical that the techniques should be more widely used, and research on these methods might well be accelerated.

VIII. Acknowledgements

The authors are indebted to the Accelerator Division of the laboratory, Drs. E. Lofgren, H. Grunder and group for their cooperation in producing appropriate heavy ion beams at the BEVALAC, to Dr. J. Lyman and group for cooperation in radiologic physics and instrumentation techniques, and to Dr. A. Chatterjee for cooperation in calculations on particle properties.

Appendix A

Range-energy Relationships.

In Figure 8 are shown range-energy relationships in water for the particles and energies of interest to heavy-particle radiography (HPR). Since the maximum energy to which the BEVALAC can accelerate ions is in excess of 2 GeV/nucleon (2000 MeV/nucleon), it is clear that for all of these particles, sufficient particle range is available for penetrating the thickest subjects of interest. While there are elaborate computer codes for exact calculations, the range-energy relationships shown in Figure 8 can be represented to better than 10% accuracy by the analytic relation,

$$E/A = 29.5\ (Z^2 R/A)^{0.604} \qquad (A\text{-}1)$$

The derivative of Eqn. (1),

$$LET_\infty = dE/dR = 17.8\ Z^{1.207}\ (A/R)^{0.396} \qquad (A\text{-}2)$$

is useful for dose calculations. The quantity Z is the particle atomic number, and A is the atomic mass number. The units for the above relations are: the particle range, R, in cm of water, energy, E, in MeV, and total energy loss rate, LET_∞, in MeV/cm (= 0.1 kev/μ).

References

1. C. A. Tobias, T. L. Hayes, H. D. Maccabee, and R. M. Glaeser, "Heavy Ion Radiography and Microscopy" in Biomedical Studies with Heavy-ion Beams, UCRL-17357, p. 108 (1967).
2. C. A. Tobias and H. D. Maccabee, "Accelerated Particles in Biological Research" in Elementary Particles: Science, Technology, and Society, Academic Press (1971).
3. A. M. Koehler, Science, 160, 303 (1968).
4. V. W. Steward and A. M. Koehler, Science, 179, 913 (1973).
5. V. W. Steward and A. M. Koehler, Radiology, 110, 217 (1974).
6. D. West and A. C. Sherwood, Nature, 239, 157 (1972).
7. D. West and A. C. Sherwood, "Non-Destructive Testing", Oct. 1973.
8. E. V. Benton, R. P. Henke, and C. A. Tobias, Science, 182, 474 (1973).
9. E. V. Benton, R. P. Henke, and C. A. Tobias, in: LBL-2016 (Lawrence Berkeley Laboratory, Berkeley, California, 1973), P. 1.
10. M. Goitein, Nucl. Instrum. Methods, 101, 509 (1972).
11. M. Goitein, J. T. Lyman, and C. A. Tobias, "Radiotherapeutic Applications of Three-Dimensional Reconstruction of Anatomic Features" (in preparation).
12. T. F. Budinger and G. T. Gullberg, "Three-dimensional reconstruction in nuclear medicine by iterative least squares and Fourier transform techniques," Lawrence Berkeley Laboratory Report LBL-2146 (1973).
13. W. H. Barkas, Nuclear Research Emulsions, Academic Press (1963).
14. W. E. Burcham, Nuclear Physics, p. 177, McGraw-Hill (1963).
15. J. D. Jackson, Classical Electrodynamics, Wiley (1962).
16. R. L. Gleischer, H. W. Alter, S. C. Furman, P. B. Price, R. M. Walker, Science 178, 255 (1972).

17. E. V. Benton, "A Study of Charged Particle Tracks in Cellulose Nitrate," USNRDL-TR-68-14 (1968).

18. H. Berger, "Track-etch Radiography: Alpha, Proton, and Neutron" (to be published in Nuclear Technology).

19. R. A. Bell, P. J. Clements, and A. Langsford, "A Non-destructive Measurement of the Fluctuations in Area Density of a Graphite Block Using a 147 MeV Proton Beam," Report AERE-R, 5732, Harwell, UKAEA, England (1968).

20. P. F. J. New, et al, "Computerized Axial Tomography with the EMI Scanner", Radiology, 110, 109 (1974).

21. "High-Energy Heavy Ion Facility (BEVALAC)" - Design Study Report, LBL-786 (1972).

Figure Legends

Figure 1. Relative transmission of monoenergetic protons as determined for graphite with a proton energy of 147 MeV (from Bell, Clements and Langsford) (19).

Figure 2. Range straggling as a function of range in water for various particles. Helium ions have about half the straggling of protons and carbon ions about 1/4 of proton straggling. There is some further improvement with still heavier ions.

Figure 3. Mean beam deflection due to multiple scattering for various ions in water. Lateral scattering for carbon ions is about four times less than for protons.

Figure 4. Particle trajectories crossing an interface (not drawn to scale).

Figure 5. Range-energy relationship for H, He, C, O, Ne and Ar in water.

Figure 6. An expanded view of the three-dimensional character of the stopping point distribution of BEVALAC ^{20}Ne particles in successive layers of Lexan. The track density is directly proportional to the opaqueness. The stack has been separated to reveal individual layers.

Figure 7. Normalized Lexan and CN detector response curves. The normalized stopping distribution producing these curves is also shown. The Lexan response is the total track opening area on both detector surfaces. The CN responses

Figure 7 (continved). are the track count on the downstream surface and the total area of the central openings of etched-through tracks. All layer positions are for the center of the layer.

Figure 8. Expanded response curve for Lexan. The shaded areas are the portions of the stopping-poing distribution that contribute to the response for the indicated layer position.

Figure 9. Illustration of contrast in response between X-ray and heavy-particle radiography.

Figure 10. The dose due to a particle fluence of 1000 particles/cm^2 as a function of particle residual range (this graph is not corrected for inelastic collisions. When these are included, the lines on the right side of the graph become somewhat elevated).

Figure 11. Longitudinal resolution tester (a) consists of a block of Lucite with variable depth grooves. In (b) and (c) are Lexan radiographs made using ^{12}C and ^{16}O beams. The fifth groove from the left, 0.2 mm thick, is clearly visible. A much better depth resolution can be achieved by actual counting of tracks in the regions of interest. Note: the incident beam traverses approximately 10 cm of H_2O before reaching the subject.

Figure 12. A lateral resolution tester (a) consisting of a block of Aluminum with variable depth triangular grooves. In (b) is edge view of a stack of cellulose nitrate plastics used to record the image of (a) using ^{16}O particles. This

Figure 12 (continued). clearly shows the three-dimensional nature of the recorded image. In (c) is shown a single layer which makes up the stack (b).

Figure 13. A model of a tumor (a) consisting of a Lucite block with a 1-cm diameter spherical cavity filled with 5% lower stopping power sugar solution. note many small air bubbles; the smallest is about 1 mm in diameter. (b) and (c) show ^{12}C radiographs in CN. Note the images of the air bubbles. (d) to (g) show radiographic image in Lexan for 2%, 3%, 4%, 5% lower stopping power of the cavity, respectively.

Figure 14. ^{16}O-produced CN radiographs show portions of a diseased human aorta with details of find structure not obtainable using conventional X-ray techniques. At bottom right is an X-ray diagnostic picture taken at 35 kVp with a 0.8 mm Al. filter.

Figure 15. The radiographic image of the F344 rat in Figure 15 produced by BEVALAC ^{20}Ne particles in Lexan. (a) through (j) show the image produced in successive layers, emphasizing the three-dimensional character of the radiograph. The Lexan layers in this exposure were alternated with cellulose nitrate layers.

Figure 16. The radiographic image of a F344 rat produced by BEVALAC ^{20}Ne particles in cellulose nitrate. One layer of the stack is shown. The rat was exposed in a water bath.

Figure 17. An X-ray of the F344 rat in Figures 15 and 16 in air. The exposure is at 45 kV, 200 mas. The three bright spots are metal suture clamps.

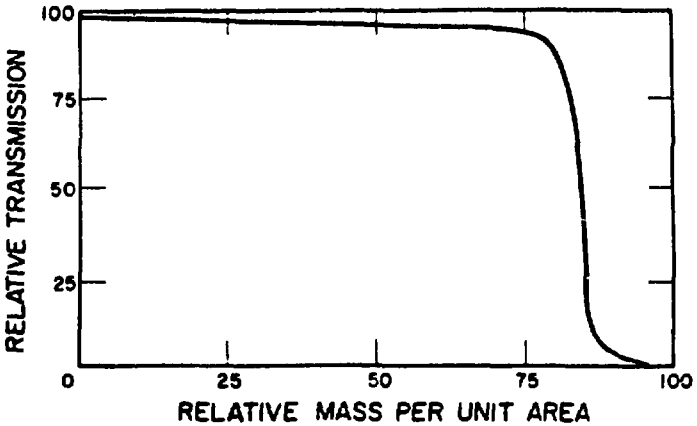

XBL 742-338

Fig. 1

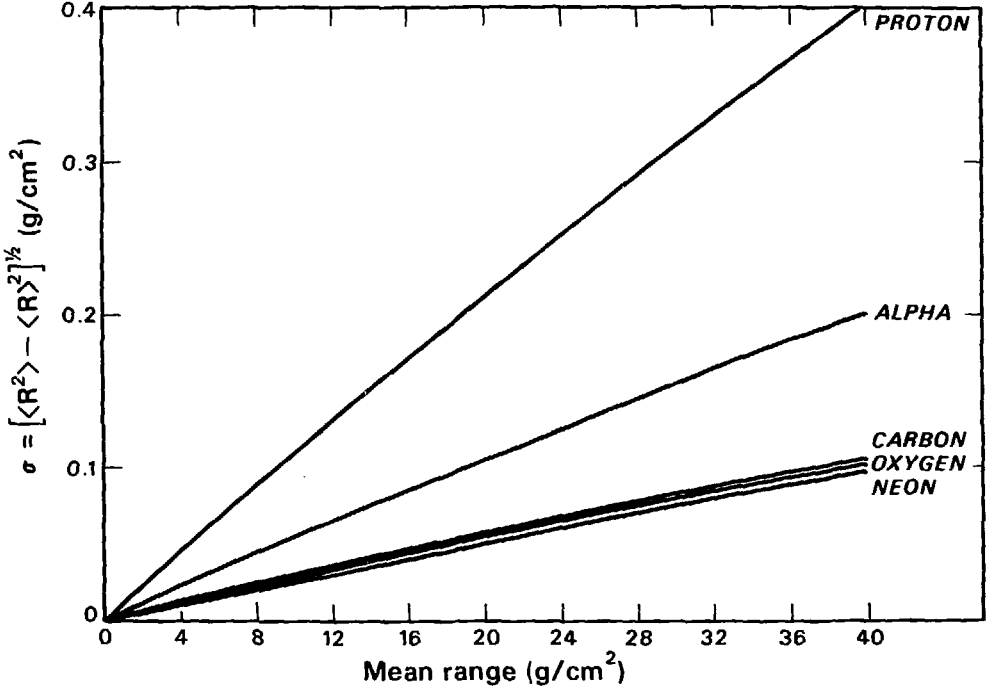

DBL 742-4642

Fig. 2

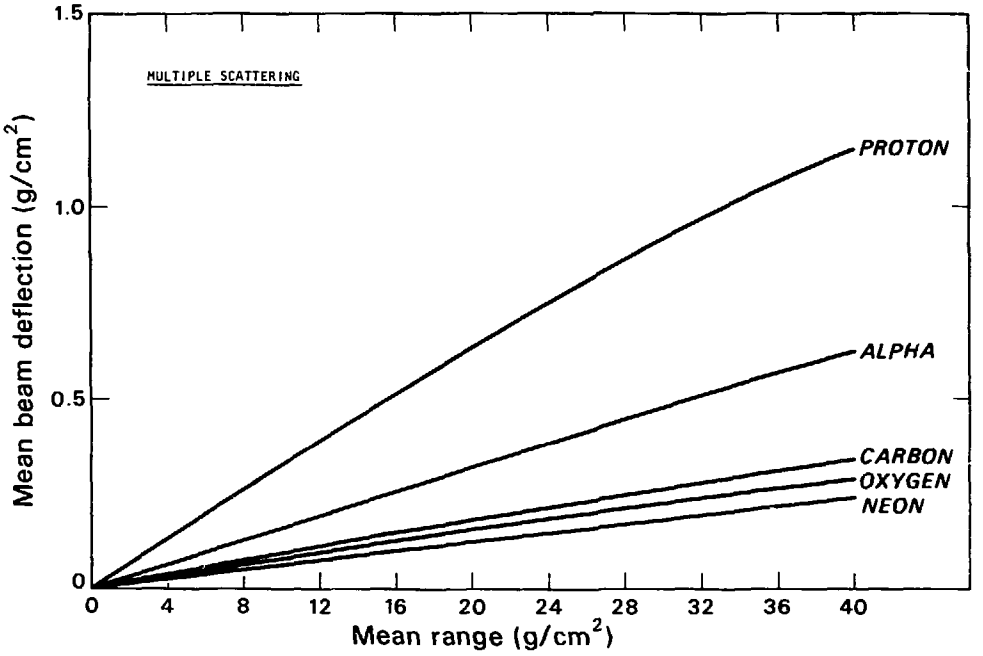

Fig. 3

DBL 741-4634

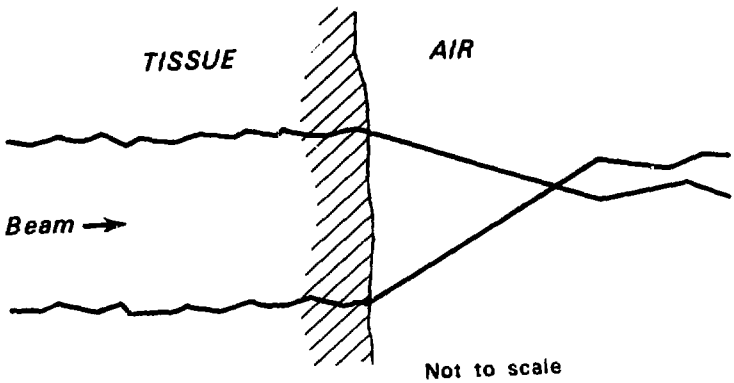

XBL 757-1760

Fig. 4

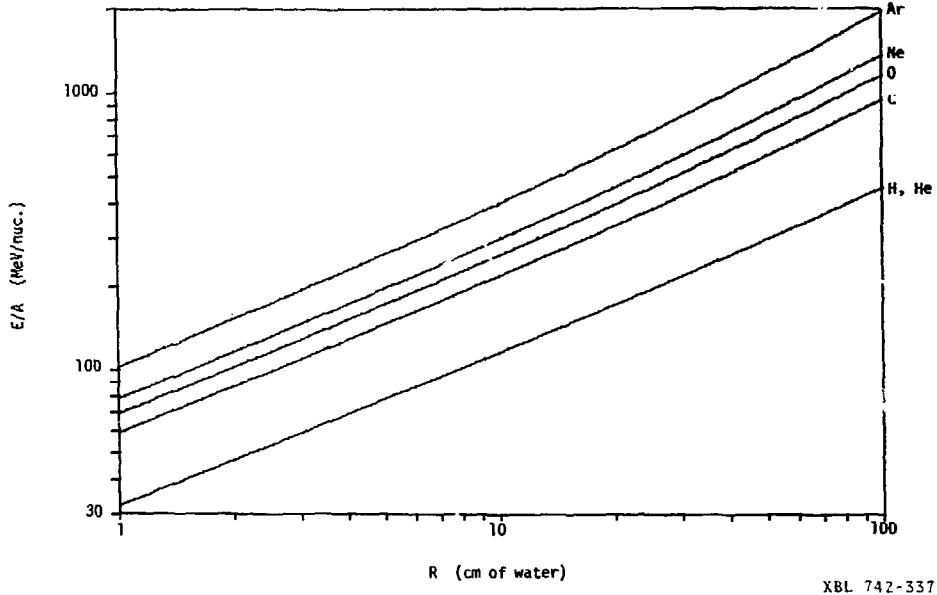
Ar
Ne
O
C
H, He
1000
100
30
E/A (MeV/nuc.)
1
10
100
R (cm of water)
XBL 742-337

Fig. 5

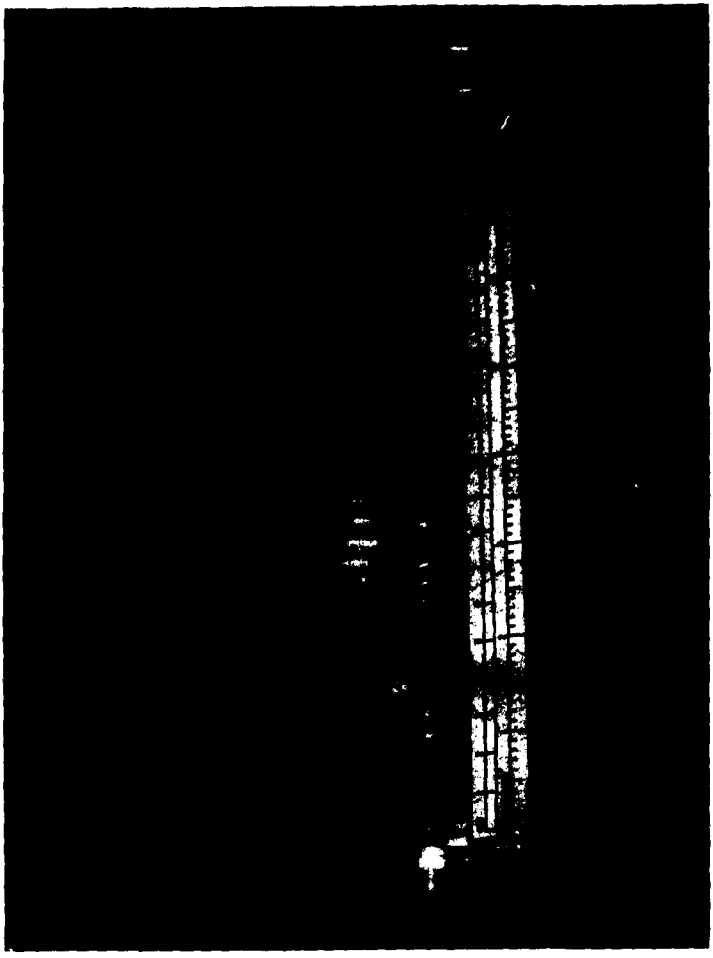

Fig. 6

CBB 751-802

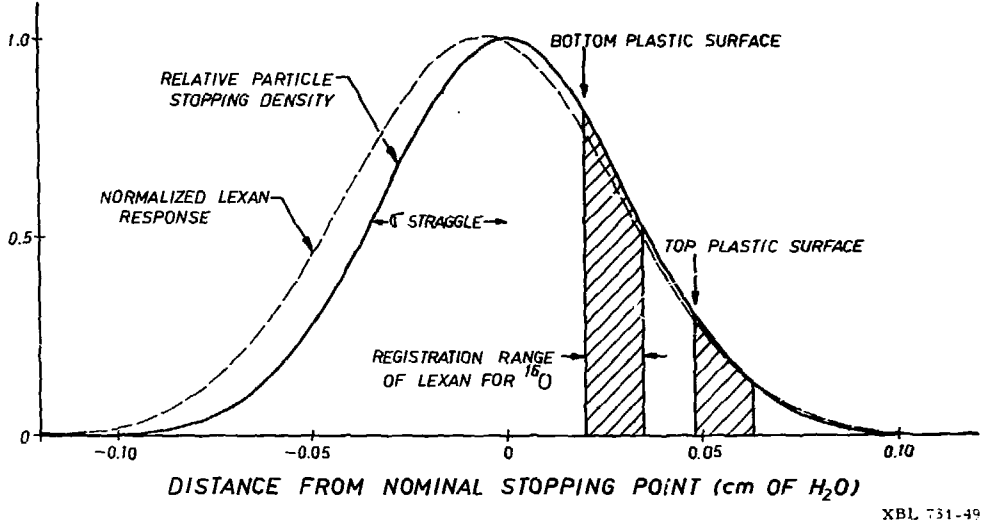
1.0
0.5
0
BOTTOM PLASTIC SURFACE
RELATIVE PARTICLE STOPPING DENSITY
NORMALIZED LEXAN RESPONSE
σ STRAGGLE
TOP PLASTIC SURFACE
REGISTRATION RANGE OF LEXAN FOR ^{16}O
−0.10
−0.05
0
0.05
0.10
DISTANCE FROM NOMINAL STOPPING POINT (cm OF H_2O)
XBL 731-49

Fig. 7

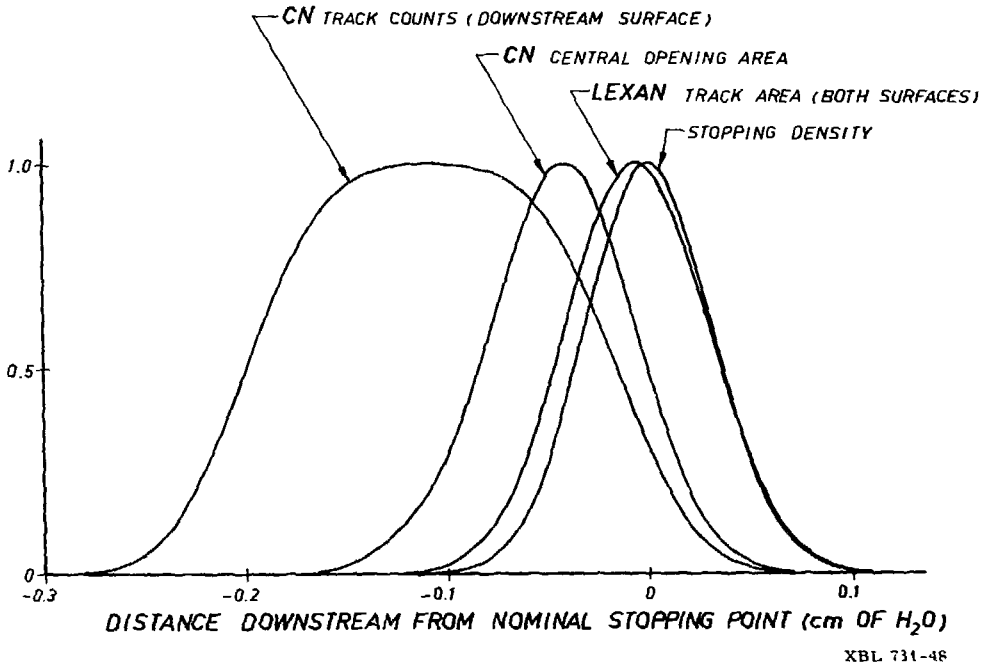
CN TRACK COUNTS (DOWNSTREAM SURFACE)
CN CENTRAL OPENING AREA
LEXAN TRACK AREA (BOTH SURFACES)
STOPPING DENSITY
1.0
0.5
0
-0.3
-0.2
-0.1
0
0.1
DISTANCE DOWNSTREAM FROM NOMINAL STOPPING POINT (cm OF H_2O)
XBL 731-48

Fig. 8

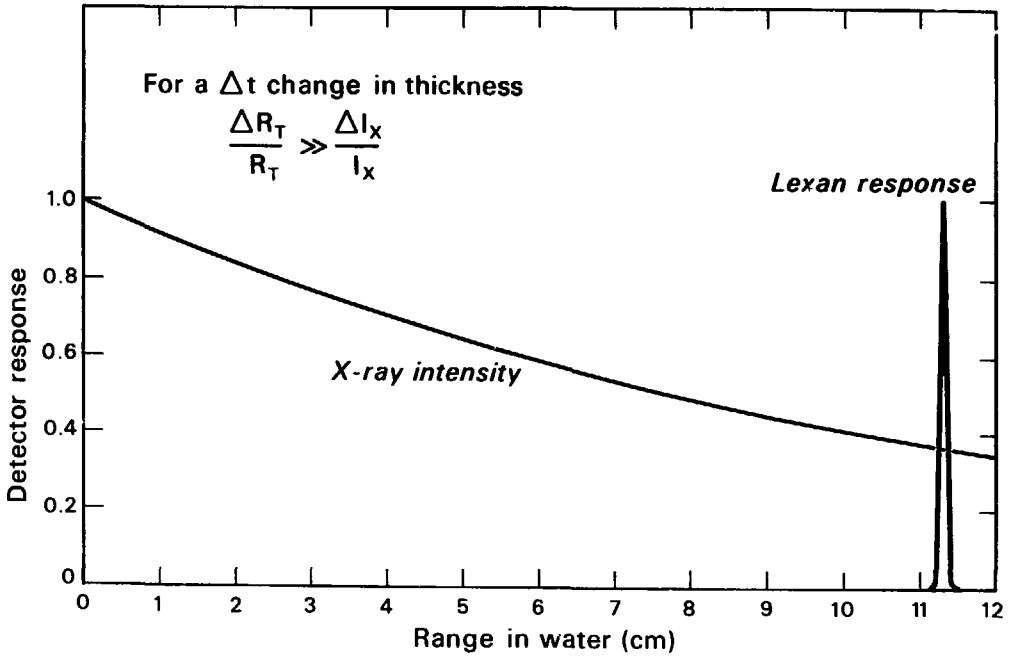

DBL 732-5053

Fig. 9

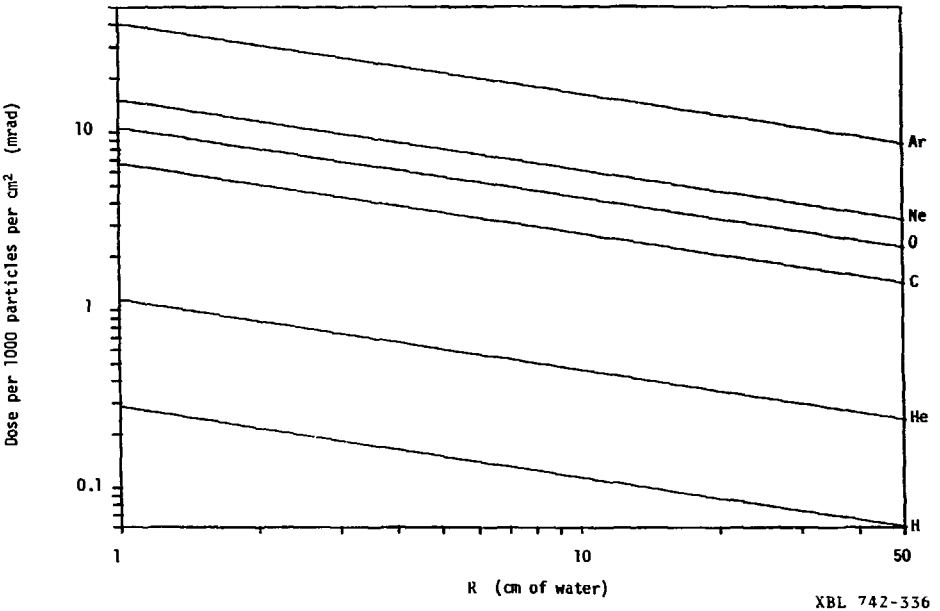
Dose per 1000 particles per cm² (mrad)
10
1
0.1
1
10
50
R (cm of water)
Ar
Ne
O
C
He
H
XBL 742-336

Fig. 10

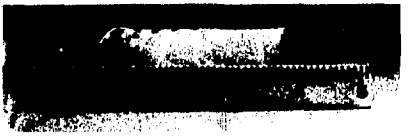

Fig. 11

XBB 741-352

Fig. 13 (d)

XBB 410-7117

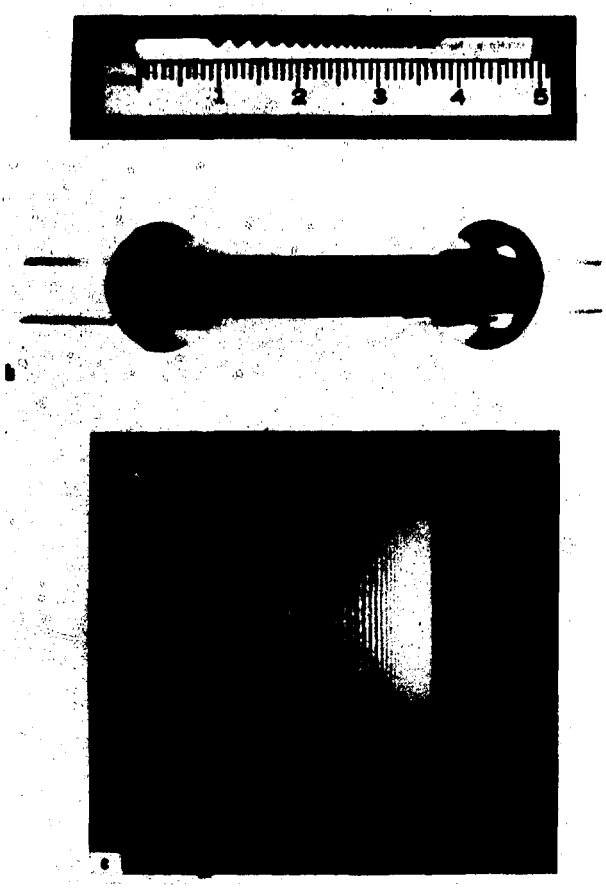

Fig. 12

XBB 741-353

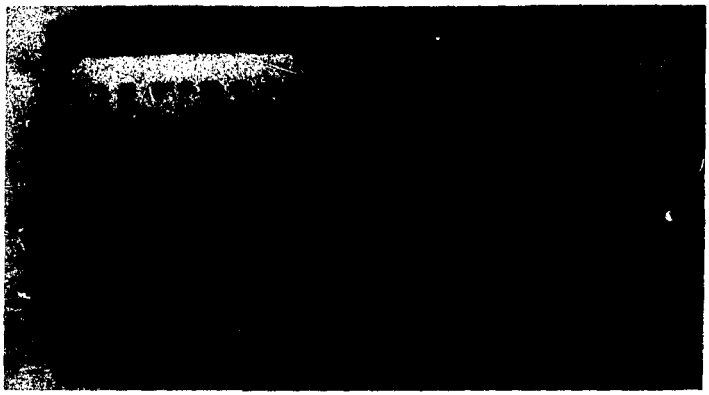

Fig. 13 (a-c)

XBB 741-351

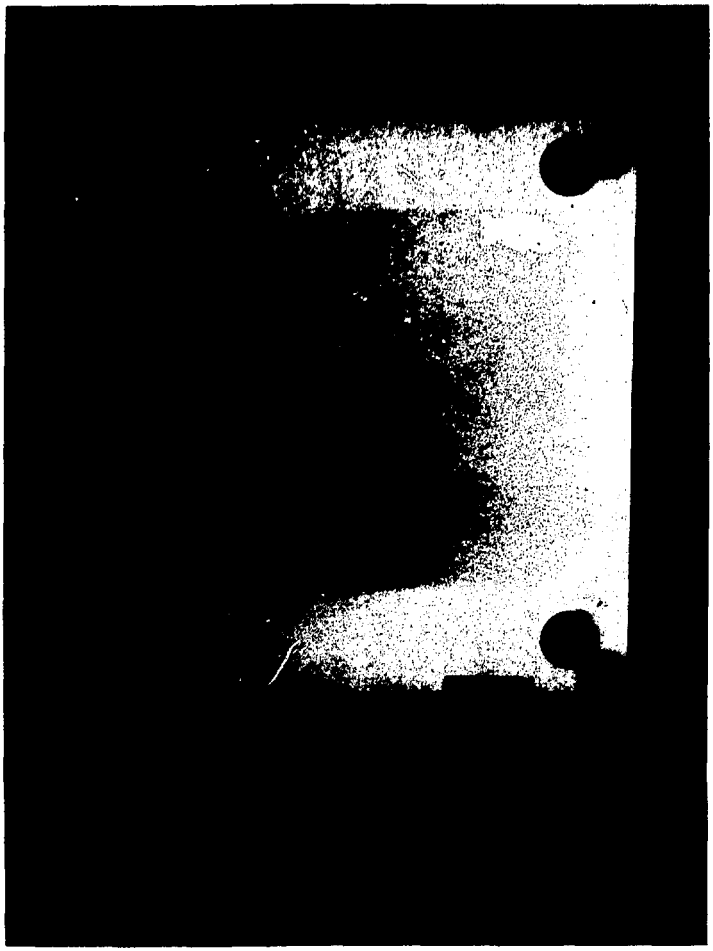

Fig. 13 (e)

XBB 7410-7119

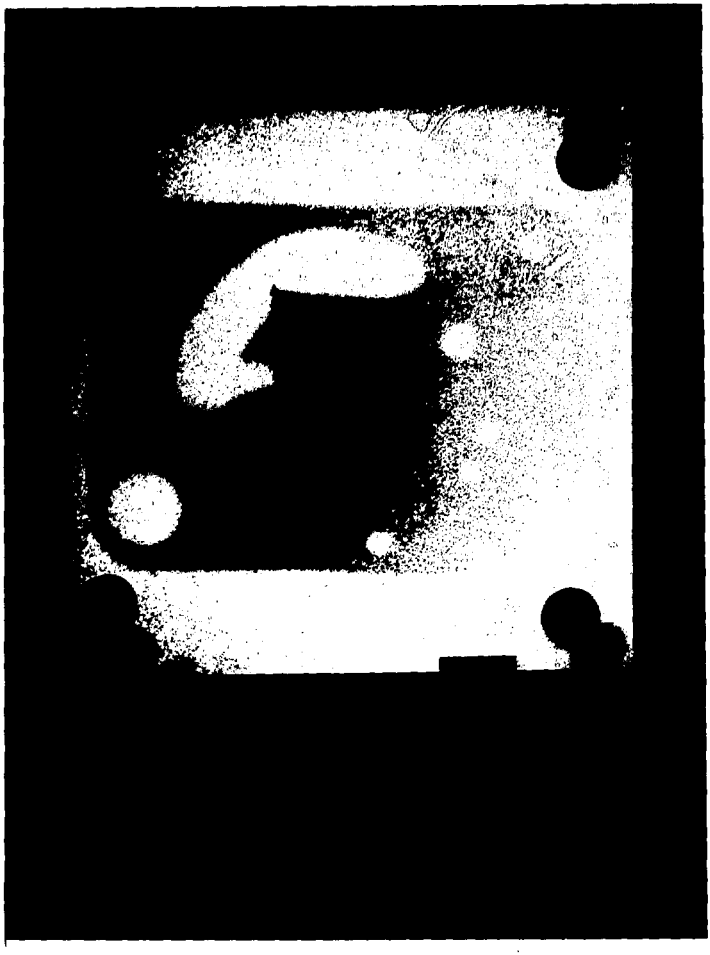

Fig. 13 (f)

XBB 7410-7118

Fig. 13 (g)

XBB 7410-7115

Fig. 14

XBB 741-354

Fig. 15 (a)

XBB 757-170

Fig. 15 (h)

XBB 731-169

Fig. 15 (c)

XBB 731-171

Fig. 15 (d)

XBB 751-172

Fig. 15 (e)

XBB 731-166

Fig. 15 (f)

XBB 751-165

Fig. 15 (g)

XBB 751-167

Fig. 15 (h) XBB 751-168

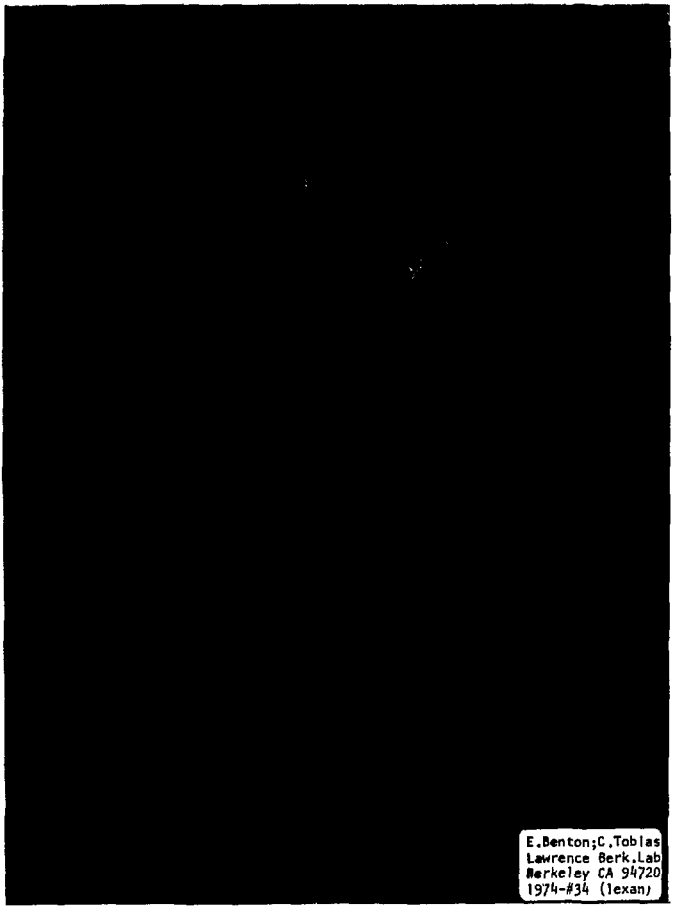

Fig. 15 (i)

XBB 751-161

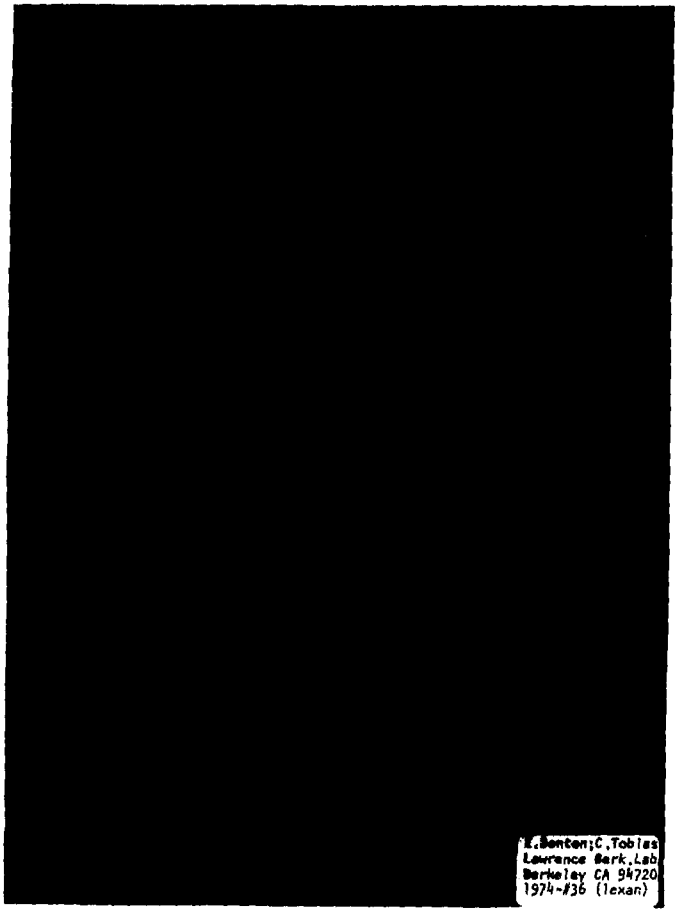

Fig. 15 (j)

XBB 751-162

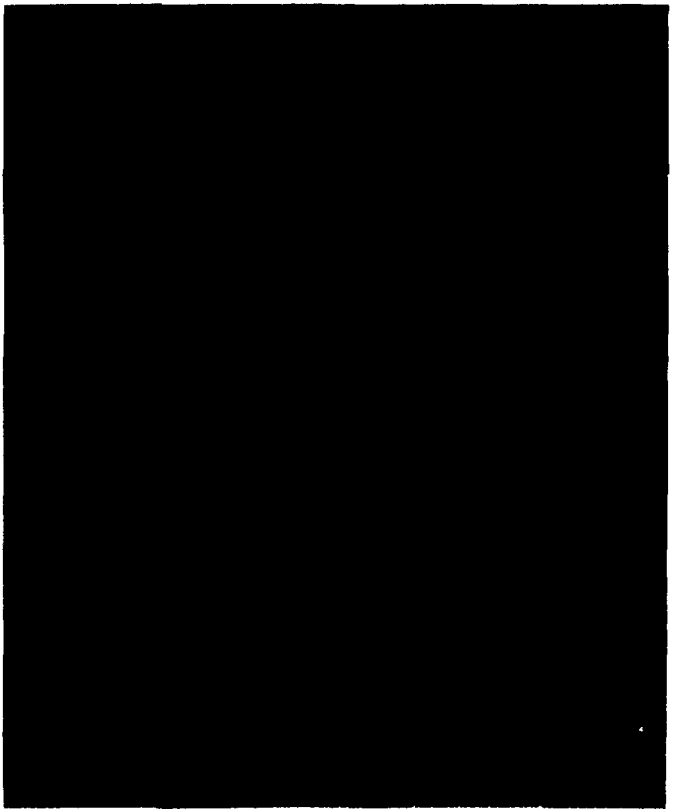

E.Benton;C.Tobias
Lawrence Berk,Lab
Berkeley CA 94720
1974-cell.nitrate

Fig. 16

XBB 751-159

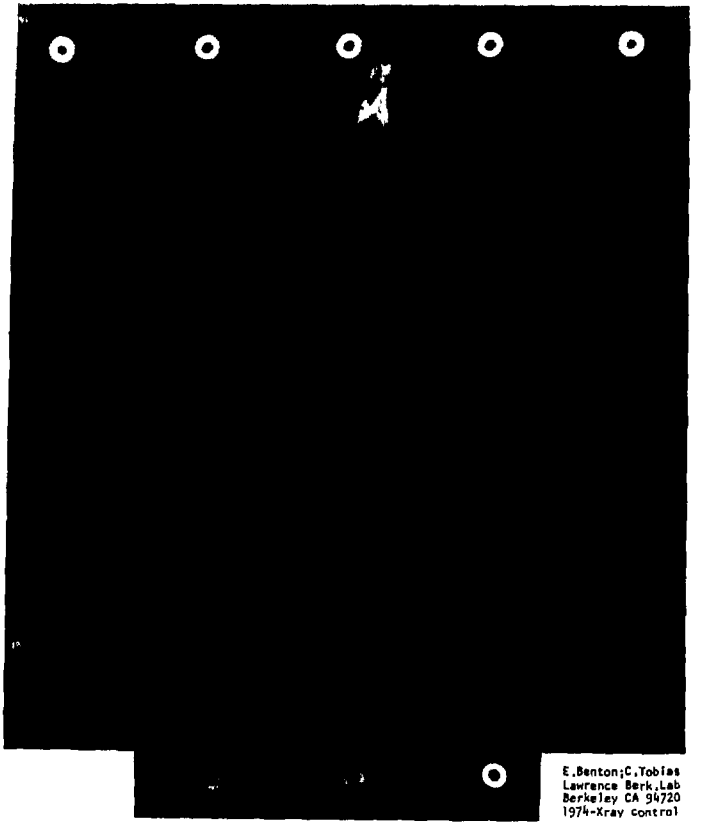

Fig. 17

XBB 751-153